On the orientation analysis of digitized images

Helmut Glünder

You wish to refer to the text or parts of it?
Then please cite according to the following bibliographic details:

Glünder H. (2013) On the orientation analysis of digitized images. *Typoscript*. Published by the author, München. – PDF-File:
<www.gluender.de/Writings/WritingsTexts/HardText.html#Gl-2013-1>

About the Author

Professor Dr.-Ing. Helmut Glünder

Born 1951, predominantly lives in München (Munich/Germany)

University Studies

Technische Universität München

- Communications Engineering, Signal Processing, and Cybernetics

Ludwig-Maximilians-Universität München

- Philosophy, Epistemology, Philosophy of Science, and Phonetics

Assistant Professor and **Research Scientist**

Institute of Communications Engineering, Technische Universität München

- Teaching all of the following research topics, and Technology & Politics of Electronic Media
- Research Mathematical Systems Theory, Biological Cybernetics, Psychophysics, Pattern Recognition, Image Analysis, Tomography, and Optical Computing

Doctorate (Dr.-Ing.)

Faculty of Electrical Engineering and Information Technology, Technische Universität München

- Thesis Geometrically Invariant Image Descriptions

Lecturer of **Applied Optics**

Fachhochschule München (University of Applied Sciences)

Senior Research Scientist

Institute of Medical Psychology, Ludwig-Maximilians-Universität München

- Teaching Medical Psychology, Sensorimotor Systems, Brain Development, and Neural Correlates of Learning
- Research Visual Motion Analysis, Sensorimotor Systems, and Theory of Olfaction

Lecturer of **Information Processing in Neural Systems**

Technische Hochschule Darmstadt

Professeur Invité of **Signal Processing and Pattern Recognition**

École Nationale Supérieure des Télécommunications de Bretagne

- Teaching Image Processing, Pattern Recognition, and Optical Signal Processing
- Research Theory of Invariant Recognition of Pictorial Patterns

Guest Lecturer of **Optical Signal Processing**

Université de Rennes I

- Teaching Fourier Optics

Lecturer of **Medical Psychology**

Ludwig-Maximilians-Universität München

Professor (Substitute) of **Neuroinformatics**

Universität Ulm

- Teaching Image Processing, Pattern Recognition, Neural Networks, and Computational Neuroscience
- Research Brain Theory, Neural Correlates of Learning, and Pulse-Coupled Neurons

Founder and **President**

Bureau of Scientific and Technologic Consulting

- Topics Acquisition, Processing and Classification of Signals and Data emphasis: Pictorial Signals and Images
- Clients Industry, Media, University, and Arts

Honorary Professor of **Computational Neuroscience**

Technische Universität Darmstadt

Further scientific activities in

Philosophy of Nature, Psychology, Theory of the Arts

More than 50 scientific original publications

On the orientation analysis of digitized images*

Helmut Glünder

Digital implementations of three mathematically equivalent approaches to global/regional orientation analysis of pictorial signals are investigated with respect to quality and cost. The efficiency of the implementations turns out to strongly depend on the image content. Hence, basic image criteria are suggested that can help with the choice of the right computing method.

Think in analog, compute in digital!

Helmut Platzer (1932-1995)

Introduction

Since the 1950s, orientation characteristics of image data were proposed for pattern recognition, among other purposes. They were commonly computed by analog electro-optic means (see references in Glünder 1986, 1993). The predominant approaches were based on integrals along straight lines through the origin of either the power spectrum or the autocorrelation function of a pictorial signal. The integral values as a function of the inclination angle of the straight line then constitute the orientation or angle feature. Interestingly, Casasent and Chang (1983) wrote: "[…] the physical significance of the two representations ([…] samples of the Fourier transform and the autocorrelation) is quite different. We make no effort to decide which is best for pattern recognition."

This view changed with the proof (Glünder 1986, 1993) that three approaches to global/regional orientation analysis of pictorial signals lead to mathematically identical results, among them the above mentioned. The significance of the finding is reflected by the much appreciated inclusion of the publication to the "Reprint collection of outstanding papers from the world literature on optical correlators" (Jutamulia 1993). Already at the time of the collection's printing however, the days of optic analog computing were numbered. When considering today's powerful digital processors, the speed advantage and the intriguing elegance of this kind of parallel processing will seldom, if ever, offset for its moderate precision and lack of flexibility. Thus, the lasting relevance of the article from 1986 is the originally intended one, namely that of its mathematical core:

- A new Fourier-theorem for two-dimensional functions (eqs. (7) and (13)).
- An alternative (eq. (10)) to the classic derivation of the Fourier projection theorem (Bracewell 1956).

Formalism

For any real-valued pictorial signal $f(x, y)$ it holds true that

$$n(\theta) = M(\theta + 90°) = p(\theta)\,,$$

where n are integrals along straight lines through the origin of the signal's autocorrelation function $a(x, y)$ depending on the inclination angle θ,[1] M are integrals along orthogonal straight lines through the origin of the signal's power spectrum $A(u,v)$, and p are integrals of squared parallel projections of the signal depending on the projection angle θ. In mathematical terms the functions can be expressed as

$$n(\theta) = \iint a(x, y)\cdot\delta(s)\,\mathrm{d}x\,\mathrm{d}y\,,$$

$$M(\theta + 90°) = \iint A(u,v)\cdot\delta(q)\,\mathrm{d}u\,\mathrm{d}v\,,\ \text{and}$$

$$p(\theta) = \int\Big[\int f(x, y)\,\mathrm{d}r\Big]^2\,\mathrm{d}s\,,$$

where $\delta(.)$ are straight delta-lines through the origin with $s = -x\sin(\theta) + y\cos(\theta)$, $r = x\cos(\theta) + y\sin(\theta)$, and $q = -u\sin(\theta + 90°) + v\cos(\theta + 90°)$. With $\mathcal{F}$ denoting the Fourier transformation one can relate

$$A(u,v) = \mathcal{F}\{a(x, y)\} = \big|\mathcal{F}\{f(x, y)\}\big|^2\,.$$

* Dedicated to the memory of my academic mentor Helmut Platzer

1 This representation is known as generalized angle chord function

Digital implementations

Obviously, the three approaches to compute what is to be called an orientation salience function (OSF)[2] involve rotations of functions in two dimensions that can easily and continuously be performed by macroscopic physical means. Not so in the virtual world of digital computers, where such functions are arrays of sample values, that is, values at spatially discrete points. In this world, reasonable representations of arbitrarily rotated functions require proper interpolation. Furthermore, rotations must be discrete as well, which raises the question of the angle increment. Not alone for these reasons, it appeared instructive to use current image processing tools for orientation analysis and to evaluate quality and computational cost of digital implementations of the approaches. Ideally suited for such investigations is the platform-independent and open source (public domain) image processing software "ImageJ" (Rasband 1997-2013; Schneider, Rasband & Eliceiri 2012) that includes, or allows one to add as plug-ins,[3] the necessary time critical routines as well as a macro language for their assembly. The computations by macros and most plug-ins are performed with double precision (64 bit).

Common to the implementations is the pre-processing of 32 bit gray-level copies of the original images that serves two purposes: The band-limited selection of a circular region of interest (ROI) and the subtraction of its mean value (DC-removal).[4] In the following, the pre-processed pictorial signals are to be called images. Another common topic is angular sampling. While orientation features, typically serving pattern recognition, often need not show the ultimate angular resolution, representations of pictorial orientations, serving unconstrained image analysis, are required to be best resolved. The necessary and sufficient angular resolution is given by the angular sampling theorem of discrete tomography (Herman 1980; Platzer 1981) that relates the number of rotation angles $\gamma \geq \frac{\pi}{2} N$ to the number N of linear independent samples, that is, picture elements (pixels), per ROI-diameter. It must be emphasized that "linear independence" implies a pictorial representation that is band-limited according to the Nyquist/Shannon-criterion. The above relation does not apply if it is violated, a situation that may occur with images that are digitally synthesized or if the bandlimit of the imaging optics is not taken into account during image acquisition.

The transformation-based approaches start with the computation of either the autocorrelation function or the power spectrum of the image. Both is accomplished by using the "ImageJ" implementation of the "Fast Fourier Transformation" (FFT). It builds upon the "Fast Hartley Transformation" and requires square-sized image supports with side lengths in pixels measuring a power of two. Within these constraints, the support size represents a free parameter. Because the FFT shows the same support size in both domains, the resolution of the transformed signal increases with the size of the support in which the image is embedded (zero-padding of the image). Power-spectral resolution or that of its re-transform, the autocorrelation function, is crucial for the computation of the line integrals in the second stage of processing. These integrals constitute the OSF and are approximated by sums of interpolated (Catmull-Rom cubic) signal values along γ diametric lines (central slices) through either the autocorrelation function or the power spectrum of the image.[5] This task is accomplished by the dedicated "ImageJ" plug-in "Slice Integrals" (Glünder 2013).

The first stage of the projection approach consists in the generation of γ projections of the image in x- and y-direction for image rotations through 90°. Although "ImageJ" provides three options for two-dimensional interpolations (nearest neighbor, linear, and Catmull-Rom cubic), the copyrighted (limited free use) plug-in "TransformJ" (Meijering 2001-2010, Meijering, Niessen & Viergever 2001) is considered for the image rotations that offers, besides others, linear, cubic B-spline, cubic O-MOMS (Blu, Thévenaz & Unser 2001), and quintic B-spline interpolation.[6] The OSF is then constituted by the sums of the squared projection values.

Methods

The following investigations are meant to deliver insights to the relationship between quality and cost of

2 If orientation analyses depend on the intensity or contrast of image structures, it appears inadequate to call the resulting functions orientation distributions, densities, or histograms, because these terms refer to a purely geometric property

3 "ImageJ" plug-ins may be copyrighted and their use may be limited

4 Added: "ImageJ" plug-in "DCfree Windowing" (Glünder 2019)

5 Cartesian-to-polar transformations are not considered

6 Interpolated image enlargements are not considered

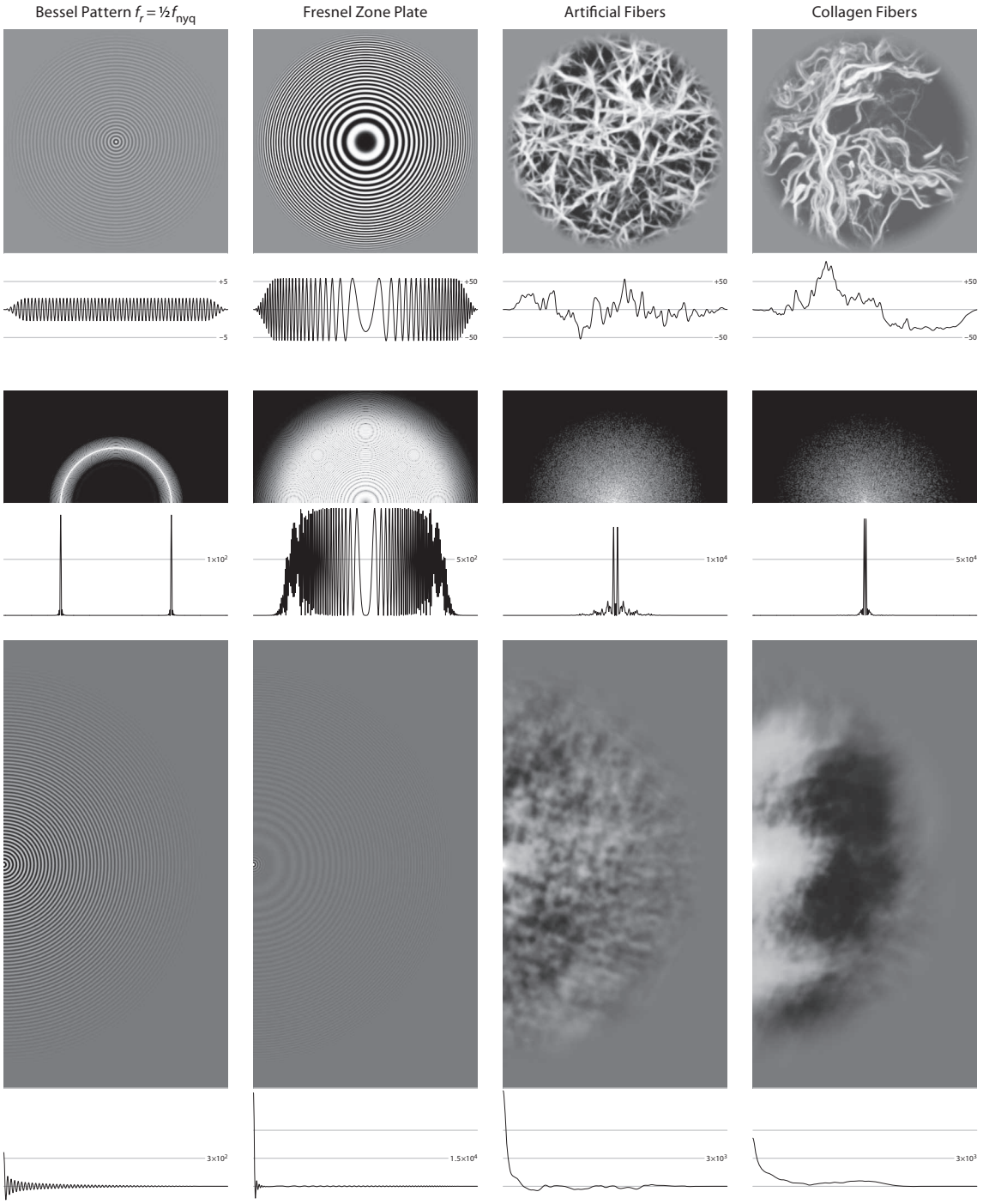

Four of the pre-processed test images (same display range and contrast enhancement) and true vertical projections (top). Top half-planes of the normalized and logarithmically scaled power spectra (six decades displayed) and true profiles along their f_x-axes (middle). Right half-planes of the normalized autocorrelation functions (same display range and contrast enhancement) and true profiles along their positive *y*-axes (bottom)

digital implementations of the three approaches for selected values of the basic parameters, namely signal resolution (over-sampling) for the transformation-based approaches and interpolation scheme for the projection approach. For this purpose, two classes of test images are considered: firstly, circular patterns, that is, radial zero-order Bessel functions of the first kind $J_0(r)$ and zone plates $\cos(\text{CONST} \cdot r^2)$; secondly, fiber images, that is, a synthesized image showing irregular fiber-like structures and a micrograph of collagen fibers. The essentially mono-frequent Bessel images are computed according to Press *et al.* (1992, p.232), with dominant radial frequencies that are 1/6, 1/3, 1/2, 2/3, and 5/6 of the Nyquist frequency. The local radial frequency of the zone plates changes linearly between zero and 5/6 of the Nyquist frequency, radially either increasing (Fresnel zone plate) or decreasing (reverse zone plate) from the center. The latter is weighted to approximately match the power spectrum of the Fresnel zone plate. Both fiber images are taken from Sage (2011-2013): The synthetic fiber image consists of the lowpass-filtered (Gauss-kernel with $\sigma = 0.9$) central part of "Artificial Fibers", and the collagen fiber image is the lowpass-filtered (Gauss-kernel with $\sigma = 1.6$) and then reduced (1/2) "Collagen-mip" micrograph.[7] While both fiber images consist of partially straight, hence clearly oriented elements, the highly artificial circular test patterns can be regarded either as containing no oriented structures at all or as showing all orientations to the same extent. The considered image size of 255×255 pixels is meant to represent global as well as regional analyses. All images are weighted by a disk-shaped window function having a 25 pixel wide raised cosine slope. Following the DC-removal, their mean gray-value is below 1 ppb of the peak value. With $N = 255$ pixels, the minimum even number of rotation angles becomes $\varkappa_{\text{even}} = 402$ that is used for all approaches.[8]

The computational cost of orientation analysis is expressed as the relative execution time of the core routines, that is, excluding image pre-processing, data post-processing, and display. It is dominated by the time required for the FFT-executions or the image interpolations, whereas the remaining computational steps, especially the slice interpolations, contribute comparably little. Three basic approaches to orientation analysis, with four parameter settings each, gives the twelve tabulated methods of OSF computation:

Approach	Power Spect.				Autocorrelation				Projection			
Parameter	8	16	32	64	4	8	16	32	linear	cubic	o-moms	quintic
Rel. Cost	1	4	16	64	1.25	5	20	80	1.33	2.67	2.67	4

Relationship between the parameters of the three approaches (over-sampling factor and interpolation scheme respectively) and the relative computational cost ±5% of the twelve associated methods

The over-sampling parameter refers to the side length of the support, in which—in case of the power spectral approach—the image, or—in case of the autocorrelation approach—its intermediately generated power spectrum is embedded. Of course, the generation of the autocorrelation function additionally requires that the image is embedded in a support of twice its side length, rounded up to a power of two.

Conventionally, OSF are normalized to their maxima, hence they assume values between a non-negative minimum and one. However, to judge the OSF quality, it appears reasonable to consider the deviation of the non-normalized data from a reference OSF of suspected high but generally not quantified quality. The root mean square of the relative deviations—the RMSD for short—suggests itself as an inverse figure of merit of orientation analysis. The computational efficiency, that is, the ratio of quality and cost, is then expressed as the inverse product of the RMSD and the relative cost.

The reference functions of perfectly circular patterns are obviously constants that are conveniently determined with high precision as the values resulting from the projection approach for $\theta = 0°$ or 90°. Their computation is neither affected by integral transformations nor by interpolations. Hence, their accuracy is only limited by the numerical precision when summing the squared values of N sums of N untransformed image samples. By applying this reference and the best transformation-based methods of analysis, the quality of the synthesized Bessel images and zone plates can be estimated.[9] The most costly transformation-based methods lead to essentially the same RMSD that, for the seven circular test patterns, is smaller than 4.6×10^{-5} (see Appendix A). Thus, the quality of both methods must be assumed considerably superior to the quality of the test images. In contrast, the projection method with quintic B-spline interpolation does not provide this quality: Although,

7 For preparation and image acquisition see Rezakhaniha *et al.* (2011)

8 Orientation angles follow the mathematical convention, that is, counter clockwise with 0° meaning horizontal

9 Precursory investigations showed that the transformation-based approaches with *linear* slice interpolation cannot reveal the quality limit of the circular test patterns. Hence, the patterns are suited to test the OSF quality of these methods with respect to reference constants

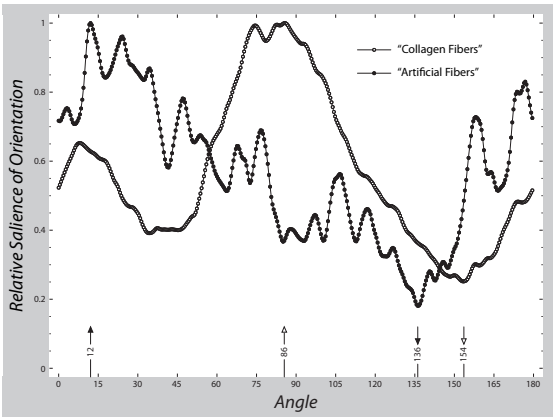

Orientation salience functions from projections of the images "Collagen Fibers" and "Artificial Fibers" using quintic B-spline interpolation

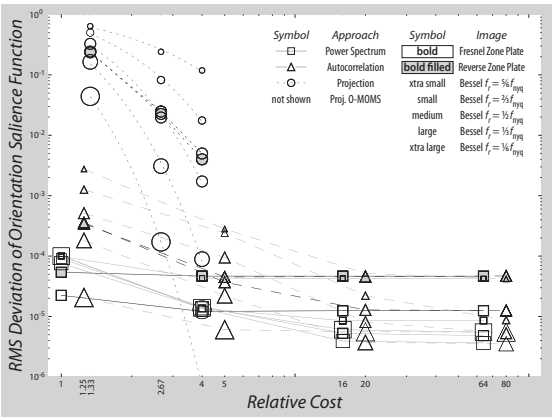

RMS deviation of orientation salience functions computed from seven circular test patterns with twelve methods. The faint dotted lines result from exponential regression, with the lowest being extrapolated

for the low frequency Bessel pattern, the RMSD of 1.3×10^{-5} roughly matches that obtained with the comparably expensive transformation-based methods, the extrapolated regression function lets one expect the pattern's quality limit of 5.5×10^{-6}.

With these insights, the usefulness of the circular test patterns may be doubted. However, if these test images are simply accepted as imperfect, mainly with respect to circularity, they can be treated alike the fiber images for which there are no ideal reference functions either. Consequently, nine of the twelve methods of orientation analysis are to be judged with respect to the OSF obtained with the most expensive method of each approach, that is, these three OSF are considered as references.

Results

The main results are about the relationship of quality and relative cost of OSF computations, where quality is to be understood as the inverse RMS deviation of the OSF from that obtained with the best of the applied methods of each approach. The decrease of the RMSD with cost is characterized by parameters of regression functions that are listed in Appendix B.

With increasing investment, the RMSD obtained from the five Bessel images decreases according to a power function of average exponent -1.5 when considering the transformation-based approaches and about exponentially with the projection methods using linear and cubic B-spline interpolation. The dependence of the OSF quality on the patterns' dominant radial frequency differs markedly with the approach. For power spectral analyses the RMSD is substantially pattern-independent and for autocorrelation analyses it varies by the average factor of 150. The pattern-dependence of the projection methods even changes with the relative cost: The RMSD varies by the factor of 14 when linear interpolation is applied and by the factor of 900 with cubic B-spline interpolation. Despite the like cost of cubic B-spline and cubic O-MOMS interpolation, the latter results in superior OSF quality. Except for the low frequency pattern, power spectral OSF computation shows the best efficiency and results in the highest OSF quality.

Because of their center frequency, both zone plates are expected to result in OSF qualities similar to those observed for the Bessel pattern of half the Nyquist frequency. In fact, this holds approximately true for the projection methods with linear and cubic B-spline interpolation, for which the RMSD decreases according to an average power of -3.6 of the relative cost. This makes the projection method with quintic B-spline interpolation significantly less efficient than its application to the Bessel pattern. With cubic O-MOMS interpolation, the RMSD is slightly higher than for the Bessel pattern. For the transformation-based approaches however, the RMSD are lower, namely about 0.26 times for the power spectral and 0.6 times for the autocorrelation approach. The minor quality differences between both zone plates must be attributed to imperfections of the spectral matching of the reverse zone plate to the Fresnel

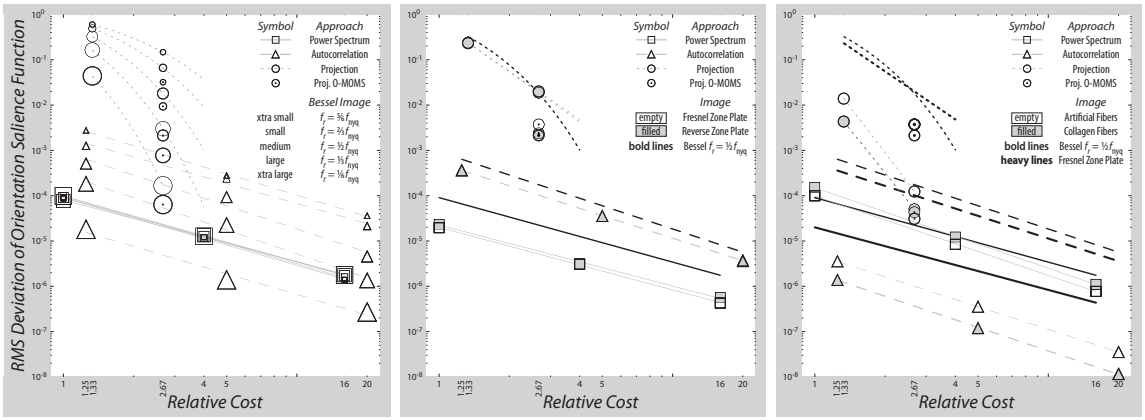

RMS deviation of orientation salience functions from that obtained with the best of the applied methods of each approach computed from five Bessel patterns (left), both zone plates (middle), and both fiber images (right). Lines are regressions by power (straight) and exponential functions (curved). Bold symbols and lines refer to the Bessel pattern of half the Nyquist frequency, heavy symbols and lines to the Fresnel zone plate

zone plate. In general, quality and efficiency of the OSF computation from the zone plates compares well with that determined for the Bessel pattern of half the Nyquist frequency. They are highest for the power spectral approach.

The RMSD of both fiber images decreases along similar lines with the relative cost. When compared to the "Collagen Fibers", the RMSD obtained for the "Artificial Fibers" is on average 2.8 times larger with the projection methods using linear or cubic B-spline interpolation (average exponent -6.6), about 0.68 times smaller with the power spectral approach, and about 2.9 times larger with the autocorrelation approach. Due to the lack of samples, it remains undecided whether the RMSD resulting from the projection approach decrease with the cost according to power or exponential functions. Compared to the two circular patterns, the OSF quality of the fiber images that results from the projection approach is up to two orders of magnitude higher. The RMSD obtained with the power spectral and autocorrelation approaches have changed places, that is, the latter results in much superior OSF quality, while the former roughly equals that of the Bessel pattern of half the Nyquist frequency. With the transformation-based approaches the exponent of the fitted power function is around -1.7 which is roughly the same as that obtained with the autocorrelation approach for the two circular patterns. With the power spectral approach applied to the circular patterns however, the RMSD decreases more slowly, that is, with an average power of -1.4 of the relative cost.

The highest quality and efficiency of the OSF computation from both fiber images is achieved with the autocorrelation approach. Even with only 4-fold over-sampling its efficiency surpasses that observed with the nearly 13 times more costly power spectral approach using 32-fold over-sampling. In general, the projection approach is considerably less efficient compared to the transformation-based approaches. With cubic O-MOMS interpolation applied to the fiber images however, it is as efficient as the power spectral method with 8-fold over-sampling.

Discussion

In essence, the OSF quality increases with the power of about 1.7 of the relative cost of the transformation-based approaches (except for power spectral analyses of circular patterns where it increases with the average power of 1.4)[10] and with a power of typically less than 7 of the cost of the projection methods with linear or B-spline interpolation (except for analyses of Bessel patterns where it increases exponentially).

To answer the crucial question of how the OSF quality depends on the image structure requires one to recall the central issue of the investigations, namely rotation-associated interpolation, be it in the usual form, as with the projection approach, or by FFT-

10 For the transformation-based approaches with *linear* slice interpolation, the OSF quality increases approximately linear with the cost (average exponent 0.99), except for power spectral analyses of circular patterns (average exponent 0.59)

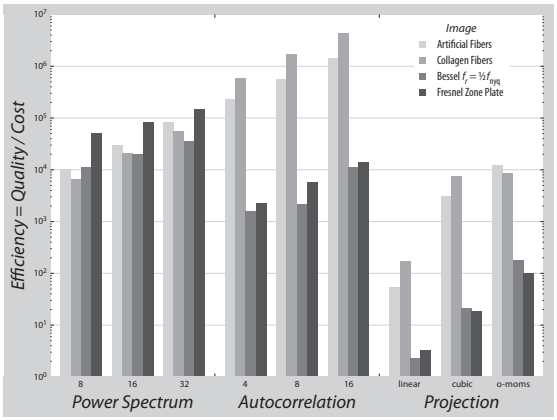

Efficiency of nine methods for the computation of orientation salience functions from two fiber images, the Bessel pattern of half the Nyquist frequency, and the Fresnel zone plate

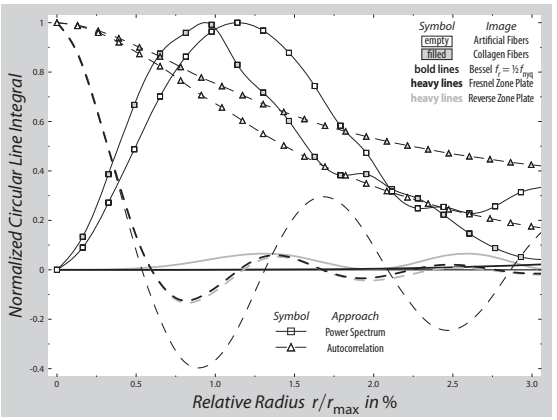

Normalized and interpolated mean radial profiles of the test images' power spectra and autocorrelation functions

interpolation (over-sampling) in conjunction with interpolated slice integration, as with the transformation-based approaches. Regarding the latter, an answer can be gained from the mean radial profile (MRP) of a pictorial signal that is dual to the OSF. It consists of the normalized values of integrals taken along concentric circles as a function of the radius. The demands are easily met by the "ImageJ" plug-in "Radial Profile" (Baggethun 2002/2009). The common center of the circles must coincide with that of the rotations. The relevant radial range is up to about one percent of the maximum radius, because interpolation errors are potentially high where the signal and the modulus of its isotropic mean gradient are high; a situation that typically occurs in the vicinity of the origin of the power spectrum and the autocorrelation function.

The first condition is not met by the power spectra of images showing pronounced bandpass behavior, such as the Bessel patterns and the zone plates. The OSF quality of power spectral orientation analyses of such images must be regarded typical for the approach. To achieve a comparable quality with arbitrary images however, their high spectral power at extremely low spatial frequencies must be carefully attenuated, an operation that may not generally be acceptable because it alters the image.

In the remaining cases, the maximum modulus of the derivative of the MRP rank-correlates near to perfectly with the RMSD, that is, inversely with the OSF quality. Of course, the MRP must be matched for the relative cost which is accomplished by expanding those of the power spectra by the factor of 1.25.

The OSF quality of the Bessel patterns definitely decreases with their dominant spatial frequency when applying the autocorrelation or the projection approach. In this regard, the OSF quality—even of arbitrary images—can be ranked by Fourier spectral characteristics, with the centroid of the MRP of the power spectrum being especially suited. The centroid frequency (tabulated as fractions of the Nyquist frequency) of the test images rank-correlates well with the RMSD, that is, inversely with the OSF quality, for all autocorrelation and projection methods.

The projection method with cubic O-MOMS interpolation leads sometimes to about the same and most often to superior OSF quality when compared to that with cubic B-spline interpolation, although they cost essentially the same. This conforms with results reported by Blu, Thévenaz and Unser (2001) who also compared their O-MOMS interpolation schemes to others by image rotations. The quality gained by using O-MOMS interpolation strongly depends on the image content but a link to basic image properties could not be found yet.

For the transformation-based approaches the relative cost generalizes well to other image sizes. However, the projection approach becomes relative more expensive with size which makes it less efficient, although the cost relations of its methods hardly grow, at least for $N > 255$.

Image	Approach	Maximum | MRP Slope |	RMSD @Cost 1.25
Bessel $f_r = ½\, f_{nyq}$	Autocorr.	0.24	5.1×10^{-4}
Reverse Zone Plate	Autocorr.	0.21	3.7×10^{-4}
Fresnel Zone Plate	Autocorr.	0.21	3.6×10^{-4}
Collagen Fibers	Power Spect.	0.17	1.0×10^{-4}
Artificial Fibers	Power Spect.	0.13	6.6×10^{-5}
Artificial Fibers	Autocorr.	0.046	3.6×10^{-6}
Collagen Fibers	Autocorr.	0.033	1.4×10^{-6}

Maximum modulus of the slope of the mean radial profiles (MRP) of power spectra and autocorrelation functions and RMS deviation of the corresponding orientation salience functions for relative cost 1.25. Rank correlation is near to perfect (Spearman's rho = 99.1%)

Image	MRP Centroid f_{centr}/f_{nyq}	RMSD AC @Cost 1.25	RMSD Proj. @Cost 1.33
Bessel $f_r = ⅚\, f_{nyq}$	0.83	2.8×10^{-3}	0.6
Bessel $f_r = ⅔\, f_{nyq}$	0.67	1.3×10^{-3}	0.49
Bessel $f_r = ½\, f_{nyq}$	0.50	5.1×10^{-4}	0.33
Reverse Zone Plate	0.39	3.7×10^{-4}	0.24
Fresnel Zone Plate	0.38	3.6×10^{-4}	0.23
Bessel $f_r = ⅓\, f_{nyq}$	0.33	1.8×10^{-4}	0.16
Bessel $f_r = ⅙\, f_{nyq}$	0.17	1.8×10^{-5}	0.044
Artificial Fibers	0.056	3.6×10^{-6}	0.014
Collagen Fibers	0.025	1.4×10^{-6}	0.0043

Normalized centroid frequency of the mean radial profiles (MRP) of power spectra, and RMS deviation of orientation salience functions computed with the low-cost autocorrelation (AC) and projection (Proj.) methods. All three rank correlations are perfect

Conclusion

The rather unexpected general outcome of the study is the complexity of digital implementations of mathematically straight-forward procedures. The intricate behavior of digital approaches to global/regional orientation analysis of pictorial signals could, to some extent, be resolved and recommendations be made of how to deal with the various methods. However, finding the optimum method for a certain class of images with respect to given computational cost requires precursory investigations that add to the cost. With the considered software tools and cost limits, the observed lower bound of the root mean square of the relative deviations of an orientation salience function from its reference function is 10^{-8}.

For orientation analyses of natural images that show an approximate $1/f_r$ (Deriugin 1956; Cohen, Gorog & Carlson 1975) or steeper decline of their amplitude spectra—a condition that is met by the "Collagen Fibers" but only poorly by the "Artificial Fibers"—the autocorrelation approach is by far the best. The power spectral approach is to be considered for orientation analyses of images with broadband amplitude spectra that decrease markedly slower than $1/f_r$. Projection methods with up to quintic spline interpolation must be ruled out for high quality or computationally efficient orientation analyses.[11]

In any case, the images need to be properly sampled, their mean value must be removed, and correct angular sampling must be applied.

Acknowledgments

I very much would like to thank Wayne Rasband for developing as well as steadily extending and supporting "ImageJ", Eric Meijering for his outstanding set of plug-ins "TransformJ", and Daniel Sage for the permission to use both fiber images.

Appendix A

Method	Image	RMS deviation
Power Spectrum @Cost 64	Bessel $f_r = ⅚\, f_{nyq}$	4.2×10^{-5}
	Bessel $f_r = ⅔\, f_{nyq}$	8.6×10^{-6}
	Bessel $f_r = ½\, f_{nyq}$	4.8×10^{-6}
	Bessel $f_r = ⅓\, f_{nyq}$	3.6×10^{-6}
	Bessel $f_r = ⅙\, f_{nyq}$	5.5×10^{-6}
	Fresnel Zone Plate	1.2×10^{-5}
	Reverse Zone Plate	4.7×10^{-5}

RMS deviation of the reference constants from the orientation salience functions as they are determined by the most costly power spectral method from the seven circular test patterns

Appendix B

Approach	Image	*a*	*b*
Projection	Bessel $f_r = ⅚\, f_{nyq}$	2.41	1.05
	Bessel $f_r = ⅔\, f_{nyq}$	3.60	1.5
	Bessel $f_r = ½\, f_{nyq}$	5.75	2.16
	Bessel $f_r = ⅓\, f_{nyq}$	8.71	2.99
	Bessel $f_r = ⅙\, f_{nyq}$	11.21	4.16

Parameters of the exponential fit $a \cdot e^{-b \cdot cost}$ applied to the RMS deviations that result from the five Bessel patterns when using the projection methods with linear and cubic B-spline interpolation

11 When applied to natural images, the projection methods with cubic interpolation (preferably O-MOMS or better) is more efficient and leads to comparable or even better results than the autocorrelation approach if *linear* slice interpolation is considered

Approach	Image	a	b	R^2
Power Spectrum	Bessel $f_r = 5/6\, f_{nyq}$	8.98×10^{-5}	1.49	0.99984
	Bessel $f_r = 2/3\, f_{nyq}$	9.72×10^{-5}	1.49	0.99995
	Bessel $f_r = 1/2\, f_{nyq}$	9.05×10^{-5}	1.42	0.99999
	Bessel $f_r = 1/3\, f_{nyq}$	7.98×10^{-5}	1.36	0.99941
	Bessel $f_r = 1/6\, f_{nyq}$	9.8×10^{-5}	1.45	0.99997
	Fresnel Zone Plate	2.00×10^{-5}	1.38	0.99992
	Reverse Zone Plate	2.25×10^{-5}	1.35	0.99968
	Artificial Fibers	9.82×10^{-5}	1.75	0.99999
	Collagen Fibers	1.5×10^{-4}	1.78	0.99998
Autocorrelation	Bessel $f_r = 5/6\, f_{nyq}$	3.75×10^{-3}	1.56	0.99983
	Bessel $f_r = 2/3\, f_{nyq}$	1.99×10^{-3}	1.47	0.99631
	Bessel $f_r = 1/2\, f_{nyq}$	9.30×10^{-4}	1.70	0.99254
	Bessel $f_r = 1/3\, f_{nyq}$	3.05×10^{-4}	1.77	0.99873
	Bessel $f_r = 1/6\, f_{nyq}$	2.17×10^{-5}	1.52	0.99812
	Fresnel Zone Plate	5.2×10^{-4}	1.66	1
	Reverse Zone Plate	5.27×10^{-4}	1.65	0.99997
	Artificial Fibers	5.15×10^{-6}	1.66	1
	Collagen Fibers	1.99×10^{-6}	1.72	0.99997
Projection	Fresnel Zone Plate	6.35×10^{-1}	3.52	
	Reverse Zone Plate	6.82×10^{-1}	3.66	
	Artificial Fibers	9.59×10^{-2}	6.77	
	Collagen Fibers	2.69×10^{-2}	6.4	

Parameters of the power fit $a \cdot \cos^{-b}$ applied to the RMS deviations that result from all test images when using the transformation-based approaches and from the zone plates and fiber images when using the projection methods with linear and cubic B-spline interpolation

References

Baggethun P. (2002/2009) *Radial Profile* [ImageJ plug-in]. Pittsburgh/PA. <https://rsb.info.nih.gov/ij/plugins/radial-profile.html>

Blu T., Thévenaz P. and Unser M. (2001) MOMS: maximal-order interpolation of minimal support. *IEEE Transactions on Image Processing* **10**: 1069-1080.

Bracewell R.N. (1956) Strip integration in radio astronomy. *Australian Journal of Physics* **9**: 198-217.

Casasent D. and Chang W.-T. (1983) Generalized chord transformation for distortion-invariant optical pattern recognition. *Applied Optics* **22**: 2087-2094.

Cohen R.W., Gorog I. and Carlson C.R. (1975) *Image descriptors for displays*. Technical Report No. AD-A007 585 (March 1975), RCA Laboratories, Princeton/NJ.

Deriugin N.G. (1956) The power spectrum and the correlation function of the television signal. *Telecommunications* **1**: 1-12.

Glünder H. (1986) Integrals along central slices through the power spectrum and the auto correlation function. *Optics Communications* **57**: 3-9.

Glünder H. (1993) Integrals along central slices through the power spectrum and the auto correlation function. In: Jutamulia S. (ed.) *Selected papers on optical correlators*. SPIE Optical Engineering Press, Bellingham/WA, pp. 655-660.

Glünder H. (2013) *Slice Integrals* [ImageJ plug-in]. Munich/Germany. <https://www.gluender.de/Miscellanea/MiscTexts/UtilitiesText.html#Gl-2013-1>

Glünder H. (2019) *DCfree Windowing* [ImageJ plug-in]. Munich/Germ. <https://www.gluender.de/Miscellanea/MiscTexts/UtilitiesText.html#Gl-2019-1>

Herman G.T. (1980) *Image reconstruction from projections. The fundamentals of computerized tomography*. Academic, New York/NY.

Jutamulia S. (ed.) (1993) *Selected papers on optical correlators*. SPIE Optical Engineering Press, Bellingham/WA.

Meijering E.H.W. (2001-2010) *TransformJ* [ImageJ plug-in]. Erasmus MC Biomedical Imaging Group, Rotterdam/Netherlands. <https://www.imagescience.org/meijering/software/transformj/>

Meijering E.H.W., Niessen W.J. and Viergever M.A. (2001) Quantitative evaluation of convolution-based methods for medical image interpolation. *Medical Image Analysis* **5**: 111-126.

Platzer H. (1981) Optical image processing. In: Oja E. and Simula O. (eds.) *The second Scandinavian conference on image analysis*. Pattern Recognition Society of Finland, Espoo/Finland, pp. 128-138.

Press W.H., Flannery B.P., Teukolsky S.A. and Vetterling W.T. ([1]1988, [2]1992) *Numerical recipes in C. The art of scientific computing*. Cambridge University Press, New York/NY.

Rasband W.S. (1997-2013) *ImageJ* [Software]. U.S. National Institutes of Health, Bethesda/MD. <https://rsb.info.nih.gov/ij/>

Rezakhaniha R., Agianniotis A., Schrauwen J.T.C., Griffa A., Sage D., Bouten C.V.C., van de Vosse F.N., Unser M. and Stergiopulos N. (2012) Experimental investigation of collagen waviness and orientation in the arterial adventitia using confocal laser scanning microscopy. *Biomechanics and Modeling in Mechanobiology* **11**: 461-473.

Sage D. (2011-2013) *OrientationJ. ImageJ's plug-in for directional analysis in images*. EPFL Biomedical Imaging Group, Lausanne/Switzerland. <http://bigwww.epfl.ch/demo/orientation/#ref>

Schneider C.A., Rasband W.S. and Eliceiri K.W. (2012) NIH Image to ImageJ: 25 years of image analysis. *Nature Methods* **9**: 671-675.